

Systematic search for VHE gamma-ray emission from X-ray bright high-frequency BL Lac objects

J. Albert^a, E. Aliu^b, H. Anderhub^c, P. Antoranz^d, A. Armada^b, C. Baixeras^e, J. A. Barrio^d, H. Bartko^f, D. Bastieri^g, J. K. Becker^h, W. Bednarekⁱ, K. Berger^a, C. Bigongiari^g, A. Biland^c, R. K. Bock^{f,g}, P. Bordas^j, V. Bosch-Ramon^j, T. Bretz^a, I. Britvitch^c, M. Camara^d, E. Carmona^f, A. Chilingarian^k, J. A. Coarasa^f, S. Commichau^c, J. L. Contreras^d, J. Cortina^b, M.T. Costado^{m,v}, V. Curtef^h, V. Danielyan^k, F. Dazzi^g, A. De Angelisⁿ, C. Delgado^m, R. de los Reyes^d, B. De Lottoⁿ, E. Domingo-Santamaría^b, D. Dorner^a, M. Doro^g, M. Errando^b, M. Fagiolini^o, D. Ferenc^p, E. Fernández^b, R. Firpo^b, J. Flix^b, M. V. Fonseca^d, L. Font^e, M. Fuchs^f, N. Galante^f, R.J. García-López^{m,v}, M. Garczarczyk^f, M. Gaug^m, M. Gillerⁱ, F. Goebel^f, D. Hakobyan^k, M. Hayashida^f, T. Hengstebeck^q, A. Herrero^{m,v}, D. Höhne^a, J. Hose^f, C. C. Hsu^f, P. Jaconⁱ, T. Jogler^f, R. Kosyra^f, D. Kranich^c, R. Kritzer^a, A. Laille^p, E. Lindfors^l, S. Lombardi^g, F. Longoⁿ, J. López^b, M. López^d, E. Lorenz^{c,f}, P. Majumdar^f, G. Maneva^r, K. Mannheim^a, O. Mansuttiⁿ, M. Mariotti^g, M. Martínez^b, D. Mazin^b, C. Merck^f, M. Meucci^o, M. Meyer^{a,*}, J. M. Miranda^d, R. Mirzoyan^f, S. Mizobuchi^f, A. Moralejo^b, D. Nieto^d, K. Nilsson^l, J. Ninkovic^f, E. Oña-Wilhelmi^b, N. Otte^{f,q}, I. Oya^d, M. Panniello^{m,x}, R. Paoletti^o, J. M. Paredes^j, M. Pasanen^l, D. Pascoli^g, F. Pauss^c, R. Pegna^o, M. Persic^{n,s}, L. Peruzzo^g, A. Piccioli^o, E. Prandini^g, N. Puchades^b, A. Raymers^k, W. Rhode^h, M. Ribó^j, J. Rico^b, M. Rissi^c, A. Robert^e, S. Rügamer^a, A. Saggion^g, T. Saito^f, A. Sánchez^e, P. Sartori^g, V. Scalzotto^g, V. Scapinⁿ, R. Schmitt^a, T. Schweizer^f, M. Shayduk^{a,f}, K. Shinozaki^f, S. N. Shore^t, N. Sidro^b, A. Sillanpää^l, D. Sobczynskaⁱ, A. Stamerra^o, L. S. Stark^c, L. Takalo^l, P. Temnikov^r, D. Tescaro^b, M. Teshima^f, D. F. Torres^u, N. Turini^o, H. Vankov^r, V. Vitaleⁿ, R. M. Wagner^f, T. Wibigⁱ, W. Wittek^f, F. Zandanel^g, R. Zanin^b, J. Zapatero^e

Received date / Accepted date

ABSTRACT

Motivated by the fact that all but two (M87, BL Lac) extragalactic sources detected so far at VHE energies belong to the so-called HBL class of high-frequency peaked BL Lac objects, a systematic scan of the compilation of X-ray blazars by Donato et al. (2001) has been performed using the MAGIC telescope. The observations took place from December 2004 to March 2006 and cover sources on the northern sky visible under small zenith distances $z_d < 30^\circ$ at culmination, constraining the declination to values between -2° and $+58^\circ$. The sensitivity of the search was planned for detecting X-ray bright ($F(1\text{keV}) > 2\mu\text{Jy}$) sources emitting at least the same energy flux at 200 GeV as at 1 keV. In order to avoid strong γ -ray attenuation close to the energy threshold, the redshift of the sources was constrained to values $z < 0.3$. Of the 14 sources observed, 1ES 1218+30.4 (for the first time at very high energies) and 1ES 2344+51.4 (strong detection in a low flux state) have been detected in addition to the known bright TeV blazars Mrk 421 and Mrk 501. For the remaining sources, we present here the 99% confidence level upper limits on the integral flux above ~ 200 GeV. A marginal excess of 3.5σ from the position of 1ES 1011+49.6 (with the largest redshift $z = 0.212$ so far reported for any extragalactic VHE source) may indicate another new source. We compare the absorption corrected γ -ray luminosities at 200 GeV with simultaneous optical, archival X-ray, and radio luminosities, to constrain the statistical properties of the sample.

Subject headings: gamma rays: observations – BL Lacertae objects: individual (1ES 0120+34.0, RX J0319.8+1845, 1ES 0323+02.2, 1ES 0414+00.9, 1ES 0806+52.4, 1ES 0927+50.0, 1ES 1011+49.6, 1ES 1218+30.4, RX J1417.9+2543, 1ES 1426+42.8, RX J1725.0+1152)

1. Introduction

Blazars are within the most extreme objects among astronomical sources. Dominated by a non-thermal continuum spectrum, covering up to 20 decades in energy, they show time variability on time scales of years down to minutes (Albert et al. 2007d) and luminosities up to 10^{47} erg cm⁻² s⁻¹. According to the unified scheme (e.g. Urry & Padovani 1995), blazars are radio-loud AGN with a small angle between the jet axis and the line of sight, which effectively boosts the observed emission. BL Lac objects differ from quasars by faint or even absent emission lines.

The spectral energy density (SED) of blazars shows two pronounced peaks, the first between

IR and hard X-rays, which is commonly believed to be synchrotron radiation of highly relativistic electrons, and the second one at γ -rays. Depending on the location of the first peak, blazars are further divided in low-frequency peaked BL Lacs (LBL, IR to optical) and high-frequency peaked BL Lacs (HBL, UV to X-rays). The second peak at high energies can be explained by inverse Compton scattering of low energy photons, produced as synchrotron radiation by the same population of electrons (Synchrotron Self Compton, SSC, Maraschi et al. (1992)), or from ambient thermal photon fields, which could enter directly into the emission region (Dermer & Schlickeiser 1993) or by scattering on material surrounding the jet (Sikora et al. 1994). There could also be an hadronic origin for the γ -ray emission, either from electro-magnetic cascades, initiated by ultra high energy protons (Mannheim 1993) or dominated by proton synchrotron radiation (Muecke & Protheroe 2001).

In December 2004, when the cycle 1 observations with the Major Atmospheric Gamma-ray Imaging Cherenkov (MAGIC) telescope started, the number of known VHE blazars was six, all of them X-ray bright HBL objects. Now the number amounts to 18, including one LBL (BL Lacertae, Albert et al. 2007e) as well as the giant radio galaxy M87 (Aharonian et al. 2006b).

The detection of VHE γ -rays from cosmological distances is aggravated, due to absorption of γ -rays by photon-photon interactions with low energy photons from the extragalactic background radiation. In fact, the redshifts of blazars detected so far above a few hundred GeV are rather low as expected from predictions of the correlation between the γ -ray attenuation and the redshift of the source, known as Fazio-Stecker relation (Fazio & Stecker 1979; Kneiske et al. 2004).

Due to the small field-of-view of an Imaging Air Cherenkov Telescope (IACT) and a duty cycle of ~ 1000 hrs per year, promising candidates for VHE emission have to be selected carefully. All established TeV sources are bright X-ray sources, most of them with comparable luminosities in both regimes, which makes a systematic scan of the X-ray brightest HBL objects reasonable. As no flux limited all-sky survey in the hard X-ray regime exist, the compilation from Donato et al. (2001) was used for the selection of the sample.

^aUniversität Würzburg, D-97074 Würzburg, Germany

^bIFAE, Edifici Cn., E-08193 Bellaterra (Barcelona), Spain

^cETH Zurich, CH-8093 Switzerland

^dUniversidad Complutense, E-28040 Madrid, Spain

^eUniversitat Autònoma de Barcelona, E-08193 Bellaterra, Spain

^fMax-Planck-Institut für Physik, D-80805 München, Germany

^gUniversità di Padova and INFN, I-35131 Padova, Italy

^hUniversität Dortmund, D-44227 Dortmund, Germany

ⁱUniversity of Łódź, PL-90236 Lodz, Poland

^jUniversitat de Barcelona, E-08028 Barcelona, Spain

^kYerevan Physics Institute, AM-375036 Yerevan, Armenia

^lTuorla Observatory, Turku University, FI-21500 Piikkiö, Finland

^mInst. de Astrofísica de Canarias, E-38200, La Laguna, Tenerife, Spain

ⁿUniversità di Udine, and INFN Trieste, I-33100 Udine, Italy

^oUniversità di Siena, and INFN Pisa, I-53100 Siena, Italy

^pUniversity of California, Davis, CA-95616-8677, USA

^qHumboldt-Universität zu Berlin, D-12489 Berlin, Germany

^rInst. for Nucl. Research and Nucl. Energy, BG-1784 Sofia, Bulgaria

^sINAF/Osservatorio Astronomico and INFN, I-34131 Trieste, Italy

^tUniversità di Pisa, and INFN Pisa, I-56126 Pisa, Italy

^uICREA & Institut de Ciències de l'Espai (IEEC-CSIC), E-08193 Bellaterra, Spain

^vDepto. de Astrofísica, Universidad, E-38206 La Laguna, Tenerife, Spain

^xdeceased

*correspondence: meyer@astro.uni-wuerzburg.de

Here the upper limits on the integral flux above ~ 200 GeV from a sample of 10 X-ray bright HBLs as well as the results of an observation of 1ES 1218+30.4 from January to March 2006 are reported. In Sect. 2 the selection criteria for this sample are discussed, while the description of the observations and the data can be found in Sect. 3. The data analysis technique will be described in Sect. 4, the analysis results are summarized in Sect. 5. A brief explanation of all corrections that were performed to the data can be found in Sect. 6. The results are discussed in the context of the SED together with archival radio and X-ray data as well as simultaneous optical data in Sect. 7.

2. HBL sample

We used the compilation from Donato et al. (2001), which provides 421 X-ray fluxes with spectral information of 268 blazars (136 of them HBL objects) together with average radio (at 5 GHz) and optical (V-band) fluxes. The selection criteria were (i) redshift $z < 0.3$, (ii) X-ray flux $F_x(1 \text{ keV}) > 2 \mu\text{Jy}$, and (iii) zenith distance (zd) $\theta < 30^\circ$ during culmination.

The selection was made to avoid strong γ -ray attenuation at the energy threshold. At $z = 0.3$, the expected cut-off energy is still above 200 GeV, where MAGIC has its highest sensitivity. As the energy threshold increases with the zenith distance, all observations were done below 40° , where the energy threshold is around 200 GeV. As most of the established TeV sources show comparable luminosities in X-rays and in γ -rays, only the X-ray brightest HBLs were selected, leading to a cut at $2 \mu\text{Jy}$. Assuming the same luminosity at ~ 200 GeV, it corresponds to $\sim 7\%$ of the flux of the Crab Nebula, which would be detectable for MAGIC within 15 hrs.

All sources should be observed for at least 15 hrs. The goal was to establish new VHE sources as well as to make a systematic view on the X-ray brightest HBL objects within a certain redshift range. The complete sample is listed in Table 1.

3. Observations

The MAGIC telescope is a single dish IACT, located on the Canary island of La Palma (28.8° N, 17.8° W, 2200 m a.s.l.). A 17 m diameter tessellated parabolic mirror with a total surface of

234 m^2 , mounted on a light-weight space frame made from carbon fiber reinforced plastic tubes, focuses Cherenkov light from air showers, initiated by γ -rays or charged cosmic rays, onto a 576-pixel photomultiplier camera with a field-of-view of 3.5° . The analogue signals are transported via optical fibers to the trigger electronics and each channel is read out by a 300 MHz FADC. Further details on the telescope can be found in Baixeras et al. (2004) and Cortina et al. (2005). Note, that the readout system is now exchanged by a ultra fast 2GSamples/s digitization system since February 2007. A second telescope of the same size for observations in stereo mode is currently under construction.

The observations took place from December 2004 to March 2006 in moonless nights. The data are taken in different observation modes. If the telescope is pointing to the source (on-mode), the background has to be determined by so-called off-data, where the telescope points to a nearby sky region where no γ -ray source is expected. The off-data cover the same zd range with a similar night-sky background light intensity. The larger fraction of the source sample was observed in the so-called wobble mode, where the telescope is pointing 0.4° away from the source. The position is changing every 20 minutes to the opposite to achieve a symmetric coverage in the camera. The background is then determined by the same shower images, but relatively to another position in the camera at the same distance from the camera centre than the source position.

Except 1ES 0927+50.0 and 1ES 0414+00.9, all objects were monitored by the KVA telescope (<http://users.utu.fi/kani/1m/index.html>) on La Palma in the optical R-band. None of the sources showed flaring activity in the optical during the MAGIC observations. The simultaneously taken, host galaxy corrected fluxes, averaged over the time of the MAGIC observations, are listed in Table 5.

4. Data analysis technique

The data were processed using the MAGIC Analysis and Reconstruction Software (MARS) (Bretz 2005a). A description of the different analysis steps can be found in Gaug et al. (2005) (including the calibration) and Bretz (2005b).

TABLE 1
LIST OF TARGETS.

Source	RA	dec	z	flux ^a	Γ^b	season	Time [h] ^c
1ES 0120+34.0	01 23 08.9	+34 20 50	0.272	4.34	1.93	2005 Aug-Sep	14.9
RX J0319.8+1845	03 19 51.8	+18 45 35	0.190	1.76 ^d	2.07	2004 Dec-2005 Feb 2005 Sep-2006 Jan	6.9 4.7
1ES 0323+02.2	03 26 14.0	+02 25 15	0.147	3.24	2.46	2005 Sep-Dec	11.4
1ES 0414+00.9	04 16 53	+01 04 54	0.287	5.00	2.49	2005 Dec-2006 Jan	17.8
1ES 0806+52.4	08 09 49.2	+52 18 58	0.138	4.91	2.93	2005 Oct-Dec	17.5
1ES 0927+50.0	09 30 37.6	+49 50 24	0.188	4.00	1.88	2005 Dec-2006 Mar	16.1
1ES 1011+49.6	10 15 04.2	+49 26 01	0.212 ^e	2.15	2.49	2006 Mar-Apr	14.5
Mrk 421	11 04 27.3	+38 12 31.8	0.030	39.4	2.96	2004 Nov-2005 Mar	25.6 ^f
1ES 1218+30.4	12 21 21.9	+30 10 37	0.182	8.78	2.34	2005 Jan 2006 Jan-Mar	8.2 ^g 14.6
RX J1417.9+2543	14 17 56.6	+25 43 25	0.237	3.58	2.25	2005 Apr-Jun	13.0
1ES 1426+42.8	14 28 32.5	+42 40 25	0.129	7.63	2.09	2005 Mar-Dec	6.1
Mrk 501	16 53 52.2	+39 45 36.6	0.034	20.9	2.25	2005 May-Jul	32.2 ^h
RX J1725.0+1152	17 25 04.4	+11 52 16	> 0.17 ⁱ	3.60	2.65	2005 Apr	5.3
1ES 1727+50.2	17 28 18.6	+50 13 11	0.055	3.68	2.61	- ⁱ	0 ^j
1ES 2344+51.4	23 47 04.9	+51 42 18	0.044	4.98	2.18	2005 Aug-2006 Jan	23.1 ^k

^a $F(1\text{ keV})$ [μJy], average value from different measurements, taken from Donato et al. (2001).

^b Γ is the spectral index for the differential spectrum (dN/dE) at 1 keV, assuming a power law

^cEffective observation time after quality selection

^dTwo measurements are above $3\mu\text{Jy}$, one below $1\mu\text{Jy}$

^eThe earlier reported redshift of 0.200 was recently revised by Albert et al. (2007g)

^fResults published in Albert et al. (2007b)

^gResults published in Albert et al. (2006b)

^hResults published in Albert et al. (2007d)

ⁱThe earlier reported redshift of 0.018 was recently revised by an u.l. (Sbarufatti et al. 2006)

^jProposed but not observed in cycle 1 due to bad weather

^kResults published in Albert et al. (2007c)

As the trigger rate strongly depends on the weather condition, only data with a rate above 160 Hz were used to ensure a high data quality.

The moments up to third order of the light distribution are used to characterise each event by a set of image parameters (Hillas 1985). For background suppression, a SIZE-dependent parabolic cut in WIDTH \times LENGTH is applied (Riegel 2005). To reconstruct the origin of the shower in the camera plane, the DISP method is employed (Lessard et al. 2001) to estimate the distance between the centre of gravity of the shower and its origin. The third moment determines the direction of the shower development. The constant coefficient ξ from the parametrisation of DISP in the original approach is replaced by $\xi_0 + \xi_1 \cdot (\text{LEAKAGE})^{\xi_2}$, LEAKAGE being the fraction of light contained in the outermost camera pixels. Thereby the truncation of the shower images at the camera border is taken into account. These coefficients were determined separately for on-off and wobble data using simulated γ -showers, which were produced by CORSIKA, version 6.023 (Heck et al. 1998; Majumdar et al. 2005) for z_d below 40° and energies between 10 GeV and 30 TeV, following a power law with a spectral index -2.6.

The cut coefficients for the background suppression were optimised using Crab Nebula data, taken at similar z_d . One set of cut coefficients was derived for data taken in on-off mode and one for wobble mode. The significance of a possible signal is determined from the distribution of the squared angular distance (ϑ^2) between the shower origin and the source position. The signal region is determined as $\vartheta < 0.23^\circ$, corresponding to slightly more than two times the γ point-spread function of the MAGIC telescope.

For observation in on-off mode, the off-data have to be scaled to match the on-data. This was done in the region $0.14 < \vartheta^2 < 0.64$, where no bias from the source is expected. For wobble observations three regions, located symmetrically on a ring around the camera centre with the same distance from the centre as the source position, were defined as background regions. The scale factor is fixed to 1/3.

For every source the statistical significance according to equation 17 from Li & Ma (1983) is calculated. The upper limit on the excess rate is de-

rived with a confidence level (c.l.) of 99%, using the method from Rolke et al. (2005), which takes also the scaling factor of the background into account. The upper limit for the excess rate is then compared to the excess rate of the Crab Nebula, which leads to an upper limit of the flux in units of the Crab Nebula flux above a certain energy threshold, assuming a Crab like spectrum. The energy threshold is here defined as the energy where the differential distribution (dN/dE vs. E) of simulated γ -ray events, surviving all cuts, peaks. Note that this threshold depends also on the spectral shape.

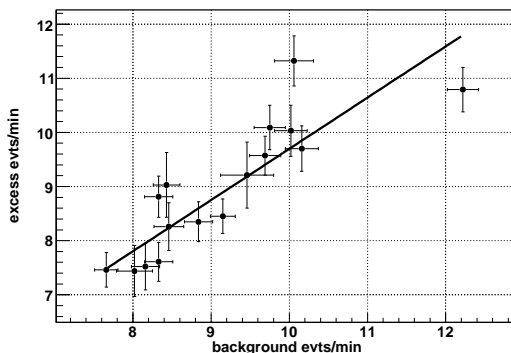


Fig. 1.— Excess rate (*excess*) vs. background rate (*bgd*) for the Crab Nebula (on-off mode). A linear fit yields $(0.95 \pm 0.10) \cdot bgd + 0.2 = excess$.

A large sample of data from the Crab Nebula in on-off as well as in wobble mode were used, spreaded over the whole observation campaign (see Table 2). This analysis showed, that the excess rate of the Crab Nebula is correlated to the background rate (after γ -hadron separation). Therefore, depending on the background rate of the AGN, a reference value for the excess rate of Crab has to be calculated. This can be understood when taking into account that even after quality selection the rates fluctuate up to 20%, depending on weather conditions. In Fig. 1 and Fig. 2 the rate of excess events vs. the background rate of different subsamples of the Crab Nebula is shown. A linear regression to the on-off samples results in an acceptable fit ($\chi^2/ndof = 26/14$), showing a clear correlation. The fit for the wobble data is quite poor ($\chi^2/ndof = 13.5/3$). As a constant fit gives even a worse result and the fit on the on-data

TABLE 2
OBSERVATIONS OF THE CRAB NEBULA USED FOR THE UPPER LIMIT CALCULATION

Season	Mode	Exp. [hrs]	Zd degr.	E_{thres} GeV	Excess [min^{-1}]	Background [min^{-1}]	scale	Sign. [σ/\sqrt{h}]
2005 Oct - 2006 Mar	w	8.6	23.0	230	6.43	6.23	0.33	14.6
2004 Dec - 2006 Mar	on	38.7	16.2	190	8.80	9.19	0.92	13.5

shows a correlation between background- and excess rate, the linear fit for the wobble data is also used to calculate the reference values for the comparison of the excess rates. The Crab units are converted into a flux of photons $\text{cm}^{-2} \text{s}^{-1}$ using the spectrum of the Crab Nebula from Albert et al. (2007f).

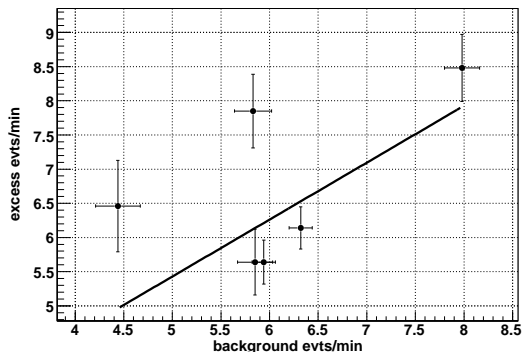


Fig. 2.— Excess rate (*excess*) vs. background rate (*bgd*) for the Crab Nebula (wobble mode). A linear fit yields $(1.26 \pm 0.3) \cdot \text{bgd} - 1.5 = \text{excess}$.

The systematic error for the flux is dominated by the error of the Crab Nebula flux, which is estimated to be $\sim 30\%$ (see Albert et al. (2007f) and discussion therein). In addition for the u.l. determination there are the uncertainties of the reference excess rate of the Crab Nebula as well as of the correct energy threshold (which depends on the source spectrum).

5. Results of the MAGIC observations

Within this observation program, VHE γ -rays were discovered from 1ES 1218+30.4 (Albert et al. 2006b) and 1ES 2344+51.5 was observed in a low flux state with high significance (Albert et al.

2007c). Mrk 421 was observed for more than 25 hrs in 2005. The results are discussed in detail in Albert et al. (2007b). Mrk 501 was observed from May to July 2005 with more than 30 hrs, revealing a high precision lightcurve on a day-by-day basis as well a two exceptionally short-time flares (see Albert et al. (2007d) for more details). For ten sources of the sample, no significant signal was seen. The 2006 observations of 1ES 1218+30.4 results in a weak signal of 4.6σ (see Sect. 5.2). A slightly refined analysis of 1ES 1011+49.6 yields a hint of a signal with a 3.5σ significance (see Sect. 5.3). The results are listed in Table 3.

5.1. Upper limits

The u.l.s are between 2.3% and 8.6% of the Crab Nebula flux. For a Crab-like spectrum the energy thresholds vary between (190 ± 15) GeV and (230 ± 15) GeV, depending on the zd of the observation. For the threshold calculation the exact zd distribution of every observation was taken into account. As the Crab spectrum at ~ 200 GeV is quite hard (spectral slope -2.26 for the differential energy spectrum), the u.l.s are also calculated for an -3.0 power law spectrum, which represents quite well the average slope of all HBLs detected at VHE so far. In Table 5 the energy threshold as well as the flux u.l. at 200 GeV is given under the assumption of a -3.0 power law.

5.2. 1ES 1218+30.4

The source was observed in 2006 from January the 29th to March the 5th during 15 nights with in total 14.6 hrs. Figure 3 shows the distribution of the squared angular distance between the reconstructed shower origin of each event and the assumed source position. The vertical line indicates the signal region. The background is determined by three off-regions in the camera. The excess

TABLE 3
RESULTS OF THE ANALYSIS.

Source	Mode	Exp. [hrs]	Zd ^a [degr.]	E_{thres} ^b [GeV]	Excess ^c	Backgr.	Scale	Sig. σ	UL c.u. ^d	UL f.u. ^e
1ES 0120+34.0	w	14.9	12.2	190	-48	5358	0.33	-0.6	0.032	0.75
RX J0319.8+1845	w	4.7	14.3	190	9	2225	0.33	0.2	0.049	1.15
RX J0319.8+1845	on	6.5	14.2	190	-95	3257	0.86	-1.2	0.033	0.78
1ES 0323+02.2	w	11.4	29.0	230	55	5262	0.33	0.7	0.064	1.16
1ES 0414+00.9	w	17.8	29.7	230	176	7309	0.33	1.8	0.057	1.03
1ES 0806+52.4	w	17.5	26.8	230	111	6174	0.33	1.2	0.056	1.01
1ES 0927+50.0	w	16.1	22.1	230	72	5721	0.33	0.8	0.052	0.94
1ES 1011+49.6	w	14.5	23.6	230	200	4857	0.33	2.5	0.086	1.55
1ES 1218+30.4	w	14.6	26.6	230	400	5423	0.33	4.6	0.073 ^f	1.31 ^f
RX J1417.9+2543	on	13.0	9.7	190	-137	9007	1.03	-1.0	0.023	0.54
1ES 1426+42.8	on	6.1	16.6	190	-7	2561	0.24	-0.1	0.050	1.18
RX J1725.0+1152	on	5.3	17.4	190	-69	2001	0.98	-1.1	0.046	1.08

^aMean zenith angle of the observation

^bPeak response energy for a Crab like spectrum

^cBackground subtracted signal events for $\vartheta < 0.23^\circ$

^dIntegral flux above the threshold given in units of the flux of the Crab Nebula (crab units, c.u.)

^eIntegral flux above the threshold given in units of f.u. = 10^{-11} photons $\text{cm}^{-2} \text{s}^{-1}$

^fIntegral flux above threshold in cu. and f.u. based on the excess rate in comparison to Crab

has a statistical significance of 4.6σ according to equ. 17 in Li & Ma (1983)(see also Table 3).

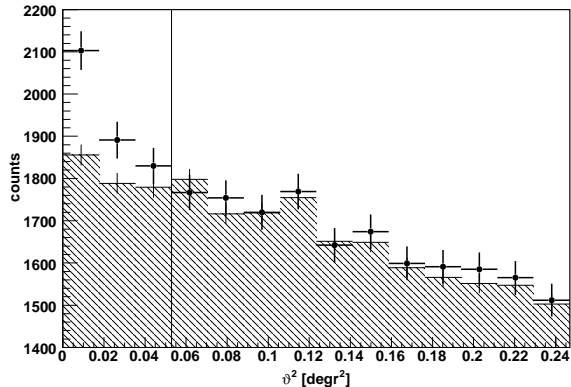


Fig. 3.— Distribution of the squared angular distance with respect to the position of 1ES 1218+30.4 (dots) and to three off-regions (scaled by 1/3, gray shaded area).

Under the assumption of a power law spectrum with spectral slope of -3.0 as measured in 2005 (Albert et al. 2006b), the energy threshold decreases with respect to a Crab like spectrum to 190 GeV. The average integral flux above 180 GeV for the complete sample is $F(> 180 \text{ GeV}) = (1.48 \pm 0.48) \times 10^{-11} \text{ photons cm}^{-2} \text{ s}^{-1}$.

The search for flux variability on time scales from days (~ 1 h observation time per night) to weeks (sample with several consecutive nights) yield no significant variability.

The integral flux above 180 GeV indicates a $\sim 30\%$ lower flux than the one measured in 2005, even though they are consistent within their errors. The average optical flux in 2006 was $\sim 20\%$ lower than in 2005, which is already significant compared to the statistical error of $\sim 2\%$. During the observations in 2006 the optical flux decreased continuously from $(1.144 \pm 0.036) \mu\text{Jy}$ on the 3rd of February to $(0.947 \pm 0.038) \mu\text{Jy}$ on the 7th of March (all optical fluxes are host galaxy subtracted). This trend continued until June, where the source remained in a low optical state. Unfortunately with six nights the sampling of the optical light curve during the MAGIC observations was quite low, hence an increase of the optical activity on a time scale of days can not be excluded.

5.3. 1ES 1011+49.6

The standard analysis performed for the whole source sample yields a significance of 2.5σ , which gives already a hint for a possible signal. In a more refined analysis, the cut in ϑ^2 , which determines the signal region, was reduced to $\vartheta = 0.20^\circ$. In case of a weak signal the increased signal to background ratio would lead to a higher significance. Also the SIZE-dependent cut for the background suppression was changed to a slightly higher value. The same analysis, performed on a data sample of the Crab Nebula, results in almost the same significance as with the standard coefficients, but with a $\sim 13\%$ lower γ -rate due to the reduced γ acceptance and a 37% lower background rate.

This analysis yields 3.5σ for 1ES 1011+49.6 which - if interpreted as a detection - corresponds to an integral flux of $F(> 180 \text{ GeV}) = (1.26 \pm 0.40) \times 10^{-11} \text{ photons cm}^{-2} \text{ s}^{-1}$. Further observations with the MAGIC telescope, triggered by an optical outburst in March 2007, shows a clear signal of 6.2σ within 18.7hrs of observation, resulting in flux $\sim 50\%$ higher than in 2006 (Albert et al. 2007g).

5.4. 1ES 1426+42.8

The VERITAS collaboration reported a steep spectrum above 300 GeV for their observations in 2001, well fitted by a power law with spectral index $-(3.50 \pm 0.35)$ (Petry et al. 2002). Extrapolating the spectral fit to 200 GeV, it yields an integral flux of 0.50 Crab above 200 GeV, which is by a factor of 10 larger than the u.l. presented in this work. Previous measurements yield a marginal detection in 2000 and upper limits for the data taken from 1995 to 1999 (Horan et al. 2002) with the most stringent one of 0.08 Crab above 350 GeV.

The HEGRA collaboration published a much harder spectrum at higher energies (above ~ 800 GeV) for their combined 1999 and 2000 data, which were well fitted by a power law with spectral index $-(2.6 \pm 0.6)$ (Aharonian et al. 2002). An extrapolation of the power law yields an integral flux above 200 GeV of 0.075 Crab. Due to the large extrapolated energy range, combined with the large statistical error of 0.6 for the slope, the uncertainty is a factor of two. Further measurements in 2002 with the HEGRA telescopes showed the source in a 2.5 times lower flux state (Aharonian et al.

2003).

The u.l. for the flux above 200 GeV presented in this work, indicate a lower flux than measured from 1999 to 2001 during several campaigns with different telescopes, whereas it is consistent with the low flux level observed in 2002.

6. Spectral Energy Distribution

The complete sample of sources, described in Sect. 2, amounts to 14 objects (without 1ES 1727+50.2) and includes the five established TeV sources Mrk 501, 1ES 1218+30.4, 1ES 1426+42.8, Mrk 421 and 1ES 2344+51.4. The overall spectral properties of this sample shall be discussed together with all other HBLs detected at VHE so far (which number amounts to ten, June 2007) in the next section. Note that all established TeV sources, which do not belong to the sample described in Sect. 2, fulfill also the criteria on redshift (except of PG 1553+113, where the redshift is not known) and X-ray flux. Therefore they also belong to the group of X-ray bright, nearby HBLs, just located at higher or lower declinations.

We collected multi-wavelength data for these 24 objects from the radio band (5 GHz, Donato et al. (2001)), the optical (R-band, 640 nm, simultaneous data from KVA or, if not available from Donato et al. (2001)), X-rays (1 keV, Donato et al. (2001)) and γ -rays (200 GeV, see Table 4, Table 5 and ref. in Table 1). For 1ES 1426+42.8, beside the u.l. derived in this work, the extrapolation of the spectrum, measured by HEGRA in 1999/2000, was used to indicate the detected flux.

The optical data are corrected for galactic extinction, using the coefficients from the NASA Extragalactic Database (NED), which are calculated following Schlegel et al. (1998).

For the γ -ray flux, sizeable attenuation is expected from current models of the evolving extragalactic (=metagalactic) background light (MRF) (Hauser & Dwek 2001; Kneiske et al. 2004). Therefore all u.l. at 200 GeV as well as the measured fluxes of the detected HBLs are corrected for the absorption, using the "best fit 2006" MRF-model from T. M. Kneiske (2007, in preparation). This model is based on the "best fit" model from Kneiske et al. (2004), but with a lower star formation rate to keep the energy density in the optical band consistent with the

u.l. derived by Aharonian et al. (2006a) from the VHE spectrum of 1ES 1101-23.3 ($z = 0.186$). The optical depth τ for all sources of this sample are listed in Table 5.

All fluxes are K-corrected. In Landt (2003), the spectral indices for the radio band, α_R^1 , of ten sources can be found. For the other 14 objects the average value $\alpha_R = 0.23$ of the ten sources is used. For the optical data, the spectral indices of nine sources, calculated at slightly higher wavelength, are taken from Bersanelli et al. (1992). For the other 15 objects the average value $\alpha_O = 0.65$ of the nine sources is used. At 1 keV, the spectral indices are taken from Donato et al. (2001), except of 1ES 0229+20.0, which is not included in this compilation. Instead the flux is taken from Costamante & Ghisellini (2002) together with the average value for the spectral index $\alpha_X = 1.36$ of all other sources. At 200 GeV the measured spectral indices are used for the detected sources, while for the non-detected ones the average value $\alpha_\gamma = 2.0$ is used. To take into account the energy dependent attenuation at VHE, which causes a hardening of the spectrum, the measured spectral indices are changed by -0.4 for $0.1 < z < 0.2$, -0.8 for $0.2 < z < 0.3$ and remain unchanged for $z < 0.1$.

After these corrections the overall spectral indices² α_{1-2} between the different energy regimes are calculated. Also the luminosities νL_ν are calculated assuming isotropic emission and with the use of the following cosmological parameters: $H_0 = 71 \text{ km s}^{-1} \text{ Mpc}^{-1}$, $\Omega_\Lambda = 0.73$, and $\Omega_m = 0.27$.

7. Discussion

We want to adress the following questions:

- Is it possible to distinguish between HBLs detected at VHE and non-detected ones concerning the spectral properties from the radio to the X-ray band?
- Is it a common property of HBLs that the luminosities at the peaks of the SED are the same, like it is expected for SSC models, assuming the same photon energy density than

¹Photon flux $F \propto \nu^{-\alpha}$ [photons $\text{cm}^{-2} \text{s}^{-1}$]

² $\alpha_{1-2} = -\log(F_1/F_2)/\log(\nu_1/\nu_2)$, $\nu_1 < \nu_2$

TABLE 4
HBLs DETECTED AT VHE WHICH DO NOT BELONG TO THE SAMPLE.

Source	F_γ^a	Ref.
1ES 1101-23.2	2.93	Aharonian et al. (2006a)
Mrk 180	11.0	Albert et al. (2006c)
PG 1553+113	11.5	Albert et al. (2007a)
1ES 1959+65.0	17.4	Albert et al. (2006a)
PKS 2005-304	6.63	Aharonian et al. (2005a)
PKS 2155-489	26.3	Aharonian et al. (2005b)
H 2356-309	2.78	Aharonian et al. (2006a)

^aFlux at 200 GeV in units of 10^{-12} erg cm⁻² s⁻¹

NOTE.—Recently the H.E.S.S. collaboration reported VHE emission from 1ES 0229+20.0, 1ES 0347-12.1 and PKS 0548-322; no fluxes were published by the time of this work.

the magnetic field density?

A general problem is the variation of the peak frequencies for different sources, while the measurements presented here are always at the same energies. In the VHE regime intrinsic peaks at several TeVs can be masked by the absorption in the MRF. As most of the data are taken non-simultaneous, another problem arises from the flux variability. From Donato et al. (2001), a typical variability at 1 keV is a factor of six for the well studied sources of the sample. Similar amplitudes can be expected at VHE.

Figure 4 shows the overall spectral index α_{RO} vs. α_{OX} for all 24 HBLs as described in the last section. The distribution is quite homogeneous. As the data are not simultaneously taken, the uncertainties due to flux variations have to be taken into account. In the case of α_{OX} a flux variability of a factor six at 1 keV corresponds to a change in the spectral index of 0.29 (if the optical flux remains the same). This is still below the difference of 0.6 between the lowest and highest values of α_{OX} for the detected VHE sources. As the variability in the radio and optical band for HBLs is lower than at X-rays or VHE γ -rays and the change of the spectral index α_{RO} is smaller for different flux ratios, the uncertainty of α_{RO} is much lower than

for α_{OX} . It is not possible to distinguish between sources detected at VHE and non-detected ones.

Figure 5 shows the overall spectral index $\alpha_{O\gamma}$ vs. $\alpha_{X\gamma}$. Both indices are distributed in a narrow band around unity for all detected sources, where $\alpha = 1$ represents the case that the energy output in both frequency bands is the same. The constraints from the u.l.s on the γ -ray flux can not exclude the region which is spanned by the detected TeV sources. In the framework of SSC models, the optical and X-ray band belong to synchrotron emission of highly relativistic electrons (first peak in the SED), while the VHE γ -rays are produced by inverse Compton scattering (second peak in the SED). If the magnetic energy density u_B is equal to the photon energy density u_{ph} , the energy output for the synchrotron and the Inverse Compton emission as well as the peak luminosities are the same. In case of HBLs, the peak frequency of the synchrotron emission is always at higher frequencies than the optical band and below 1 keV for most of them (except the extreme blazars with a hard spectrum at 1 keV). At VHE energies, most of the detected sources show a steep spectrum above ~ 200 GeV, indicating peak energies below 100 GeV. Due to absorption of VHE γ -rays in the MRF, the intrinsic peak energies could also reach

TABLE 5

UPPER LIMITS ON THE γ -RAY FLUX AT 200 GeV UNDER THE ASSUMPTION OF A -3.0 POWER LAW SPECTRUM TOGETHER WITH THE OPTICAL DEPTH AND THE SIMULTANEOUS OPTICAL DATA.

Source	Mode	$E_{\text{thres}}^{\text{a}}$ GeV	F_{γ}^{b}	τ	F_{o}^{c}	F_{X}^{d}
1ES 0120+34.0	w	170	4.0	0.53	0.47 ± 0.05	10.5
RX J0319.8+1845	w	170	4.2	0.32	0.48 ± 0.10	4.3
RX J0319.8+1845	on	170	6.2	0.32	0.14 ± 0.10	4.3
1ES 0323+02.2	w	190	8.7	0.22	1.82 ± 0.19	7.8
1ES 0414+00.9	w	190	7.7	0.57	...	12.1
1ES 0806+52.4	w	190	7.6	0.21	8.00 ± 0.23	11.9
1ES 0927+50.0	w	170	7.1	0.31	...	9.7
1ES 1011+49.6	w	170	$10.9/6.5^{\text{e}}$	0.37	11.49 ± 0.13	5.2
1ES 1218+30.4 ^f	on	120	10.1	0.29	6.13 ± 0.13	21.2
1ES 1218+30.4	w	190	7.7	0.29	4.99 ± 0.11	21.2
RX J1417.9+2543	on	140	2.5	0.43	2.11 ± 0.29	8.7
1ES 1426+42.8	on	140	5.5	0.19	1.87 ± 0.15	18.5
RX J1725.0+1152	on	190	6.3	0.27^{g}	13.27 ± 0.09	8.7
1ES 2344+51.4 ^h	w	180	11.5	0.05	3.37 ± 0.25	12.0

^aPeak response energy for a power law spectrum with index -3.0

^b $F(200 \text{ GeV})$ in units of $10^{-12} \text{ erg cm}^{-2} \text{ s}^{-1}$

^cHost galaxy subtracted flux at $4.69 \times 10^{14} \text{ Hz}$ in units of $10^{-12} \text{ erg cm}^{-2} \text{ s}^{-1}$

^dMean flux at 1 keV in units of $10^{-12} \text{ erg cm}^{-2} \text{ s}^{-1}$ taken from Donato et al. (2001)

^eFlux under the assumption of a detection

^fValues from Albert et al. (2006b)

^gFor a redshift of 0.17

^hValues from Albert et al. (2007c)

several TeV for sources located at higher redshift. In that context, the scattering of $\alpha_{O\gamma}$ and $\alpha_{X\gamma}$ around unity could be explained by a continuous distribution of peak frequencies for HBL, while the measurement was fixed at certain energies.

Figure 6 shows the overall spectral index $\alpha_{X\gamma}$ vs. X-ray luminosity $\nu_X L_X$. The average energy output at 1 keV never exceeds significantly the one at 200 GeV ($\alpha_{X\gamma} > 0.97$). For half of the detected sources, the energy output in these bands is almost the same ($\alpha_{X\gamma} \cong 1$), while for the other ones the energy output at 200 GeV is significantly lower. There is a tendency that this effect shows up at higher X-ray luminosities. For four of the ten u.l., $\alpha_{X\gamma} = 1$ can not be excluded, while for the other six sources $\alpha_{X\gamma}$ has to be higher than unity. For the non-detected sources of the sample, further observations with longer exposures are needed to reach the $\alpha_{X\gamma} = 1.10$ -line (corresponding to a seven times lower output at 200 GeV compared to 1 keV), which includes all HBLs detected at VHE so far. Note that if $\alpha_{X\gamma} = 1$ for the peak frequencies is valid, the tendency of increasing $\alpha_{X\gamma}$ values with increasing luminosities at 1 keV could be interpreted as a shift of the Inverse Compton peak to lower values.

Figure 7 shows the luminosity $\nu_\gamma L_\gamma$ at 200 GeV vs. the redshift. All detected sources are above or within the line that marks the corresponding luminosity to a flux of $2 \mu\text{Jy}$ at 1 keV. With higher redshift the absorption of γ -rays in the MRF becomes more and more dominant, resulting in an up to two times higher intrinsic flux ($z = 0.3$) than the measurable one.

The selection criterium for the declination of the sample leads to a patch of the sky with the size of 5.55 sr (or 44% sky coverage). To compare the u.l. for the total flux at 200 GeV with the diffuse Extragalactic Background Light (EBL) as measured by EGRET (Strong et al. 2004), we sum the flux over our sample except Mrk 421 (13 sources), which was seen as a point source by EGRET. Extrapolated to the complete sky, this results in $F(200 \text{ GeV}) < \epsilon \times 8.06 \times 10^{-6} \text{ MeV cm}^{-2} \text{ s}^{-1} \text{ sr}^{-1}$, where ϵ is a factor < 1 , that describes the incompleteness of the sample. The differential spectrum as measured by EGRET was well fitted by a power law with a spectral slope of -2.33 in the range from 50 MeV to 10 GeV. An extrapolation of the power law yields $F(200 \text{ GeV}) =$

$1.19 \times 10^{-4} \text{ MeV cm}^{-2} \text{ s}^{-1} \text{ sr}^{-1}$, which is ~ 15 times higher than the u.l. derived from our sample of X-ray bright HBLs. The HBL sample studied here is not complete. We know about two sources, not included in this calculation (1ES 1727+50.2 and 1ES 0229+20.0). There are also 5 HBLs from Donato et al. (2001) that fulfill the criteria of declination and X-ray flux, but are located at higher redshifts. As the absorption at 200 GeV becomes stronger above $z = 0.3$, the direct contribution of these sources should be very small. With respect to the sky coverage of some 50% of the *Einstein* Slew Survey (Elvis et al. 1992), where most of the sources of our sample belong to, we use $\epsilon \geq 0.5$, leading to an u.l. for the total flux at 200 GeV that could account for up to 13.5% of the power-law extrapolated EGRET flux. Note that the flux u.l. of our sample is already dominated by Mrk 501, which would mean that even twice the number of sources would not necessarily lead to a two times higher u.l. for the EBL. Recently Kneiske & Mannheim (2007) showed that HBLs could contribute up to 30% to the EBL at GeV energies, when including the cascade emission from higher redshifts.

8. Conclusions

The search for VHE γ -ray emission from a systematic selected sample of X-ray bright HBL objects leads to the discovery of 1ES 1218+30.4 as well as to a detection of the already established VHE source 1ES 2344+51.4 in a state of low activity with high significance (Albert et al. 2007c). For ten sources no significant signal was seen, resulting in upper limits on their integral flux above $\sim 200 \text{ GeV}$ between 2.3% and 8.6% of the Crab Nebula flux on a 99% confidence level. There is a hint for a signal for 1ES 1011+49.6 on a 3.5σ level, which is now confirmed as a source of VHE γ -rays by a second observation campaign, triggered by an high optical state (Albert et al. 2007g).

With fixed-schedule observations a bias to flaring emission states was avoided, tacitly assuming that the duty cycle of flares is short when compared with the exposure time. In spite of favoring for quiescence emission, a number of sources was detected. The upper limits obtained for the other sources still lie in a region of parameter space bracketed by the detected sources, and cor-

responding to a VHE energy flux on the level of the X-ray energy flux. It thus seems to be a question of time that more sensitive telescopes, and in particular those with a lowered energy threshold such as MAGIC-II, will eventually lead to a detection of all known bright HBLs.

The detected sources deviate in no apparent pattern from the so-far non-detected sources. A spectral shape with two equal-height bumps is expected in Synchrotron Self Compton models for the case of balanced energy densities of photons and the magnetic field. The dispersion in the distribution of the X-to- γ -ray luminosity ratio (the lowest X-to- γ -ray luminosity ratio of a detected HBL is 1/7) would then reflect variations of the peak position w.r.t. the observed band or variability, which has a sufficient amplitude in X-rays.

We would like to thank the IAC for the excellent working conditions at the Observatorio del Roque de los Muchachos in La Palma. The support of the German BMBF and MPG, the Italian INFN and the Spanish CICYT is gratefully acknowledged. This work was also supported by ETH Research Grant TH 34/04 3 and the Polish MNiI Grant 1P03D01028.

REFERENCES

- Aharonian, F., Akhperjaan, A., Barrio, J., et al. 2002, *A&A*, 384, L23
- Aharonian, F., Akhperjaan, A., Beilicke, M., et al. 2003, *A&A*, 403, 523
- Aharonian, F., Akhperjanian, A., Aye, K.-M. et al. 2005a, *A&A*, 430, 865
- Aharonian, F., Akhperjanian, A., Aye, K.-M. et al. 2005b, *A&A*, 436, L17
- Aharonian, F., Akhperjanian, A. G., Bazer-Bachi, A. R. et al. 2006, *Nature*, 440, 1018
- Aharonian, F., Akhperjanian, A. G., Bazer-Bachi, A. R. et al. 2006, *Science*, 314, 1424
- Albert, J., Aliu, E., Anderhub, H., et al. 2006a *ApJ*, 639, 761
- Albert, J., Aliu, E., Anderhub, H., et al. 2006b *ApJ*, 642, L119
- Albert, J., Aliu, E., Anderhub, H., et al. 2006c *ApJ*, 648, L105
- Albert, J., Aliu, E., Anderhub, H., et al. 2007a, *ApJ*, 654, L119
- Albert, J., Aliu, E., Anderhub, H., et al. 2007b, *ApJ*, 663, 125
- Albert, J., Aliu, E., Anderhub, H., et al. 2007c, *ApJ*, 662, 892
- Albert, J., Aliu, E., Anderhub, H., et al. 2007d, accepted by *ApJ*, arXiv:astro-ph/0702008
- Albert, J., Aliu, E., Anderhub, H., et al. 2007e, submitted to *ApJ*, arXiv:astro-ph/0703084
- Albert, J., Aliu, E., Anderhub, H., et al. 2007f, submitted to *ApJ*, arXiv:0705.3244v1 [astro-ph]
- Albert, J., Aliu, E., Anderhub, H., et al. 2007g, submitted to *ApJ*, arXiv:0706.4435 [astro-ph]
- Baixeras, C., Bastieri, D., Bigongiari, C., et al. 2004, *Nucl. Instrum. Meth.*, A518, 188
- Bersanelli, M., Bouchet, P., Falomo, R. & Tanzi, E. G. 1992, *AJ*, 104, 28
- Bretz, T. 2005a, in *AIP Conf. Proc.* 745, 730
- Bretz, T. 2005b, *Proc. of the 29th ICRC*, Pune, India
- Cortina, J., Armada, A., Biland, A., et al. 2005, *Proc. of the 29th ICRC*, Pune, India, astro-ph/0508274
- Costamante, L. & Ghisellini, G. 2002, *A&A*, 384, 56
- Dermer, C. D. & Schlickeiser, R. 1993, *ApJ*, 416, 458
- Donato, D., Ghisellini, G., Tagliaferri, G. & Fosfati, G. 2001, *A&A*, 375, 739
- Elvis, M., Plummer, D., Schachter, J. & Fabbiano, G. 1992, *ApJS*, 80, 257
- Fazio, G.G., Stecker, F.W. 1979, *Nature*, 226, 135
- Gaug, M., Bartko, H., Cortina, J. & Rico, J. 2005, *Proc. of the 29th ICRC*, Pune, India, astro-ph/0508274

- Hauser, M.G. & Dwek, E. 2001, *ARA&A*, 39, 249
- Heck, D., Knapp, J., Capdevielle, J. N., Schatz, G. & Thouw, T. 1998, Report FZKA 6019, Forschungszentrum Karlsruhe; http://www-ik.fzk.de/~heck/corsika/physics_description/corsika_physics.html
- Hillas, A. M. 1985, Proc. of the 19th ICRC, La Jolla, 3, 445
- Horan, D., Badran, H. M., Bond, I. H., et al. 2002, *ApJ*, 571, 753
- Kneiske, T. M., Bretz, T., Mannheim, K. & Hartmann, D.H. 2004, *A&A*, 413, 807
- Kneiske, T. M. & Mannheim, K. 2007, accepted by *A&A*, arXiv:0705.3778v1
- Landt, H. 2003, phd thesis, Hamburg
- Lessard, R.W., Buckley J. H., Connaughton, V. & Le Bohec, S. 2001, *Astroparticle Physics*, 15, 1
- Li, T. & Ma, Y. 1983, *ApJ*, 272, 317
- Majumdar, P., Moralejo, A., Bigongiari, C., Blanch, O. & Sobczynska, D. 2005, Proc. of the 29th ICRC, Pune, India, astro-ph/0508274
- Mannheim, K. 1993, *A&A*, 269, 67
- Maraschi, L., Ghisellini, G., & Celotti, A. 1992, *ApJ*, 397, L5
- Muecke, A. & Protheroe, R. J. 2001, *Astropart. Phys.* 15, 121
- Petry, D., Bond, I.H., Bradbury, S. M. 2002, *ApJ*, 580, 104
- Riegel, B. Bretz, T. et al. 2005, Proc. of the 29th ICRC, Pune, India
- Rolke, W., Lopez, A., Conrad, J. & James, F. 2005, *Nucl.Instrum.Meth.*, A551, 493
- Sbarufatti, B, Treves, A., Falomo, R. et al. 2006, *AJ*, 132, 1
- Schlegel, D. J., Finkbeiner, D. P. & Davis, M. 1998, *ApJ*, 500, 525S
- Sikora, M. , Begelmann, M. C. & Rees, M. J. 1994, *ApJ*, 421, 153
- Strong, A. W., Moskalenko, I. V. & Reimer, O. 2004, *ApJ*, 613, 956
- Urry, C. M. & Padovani, P. 1995, *PASP*, 107, 803

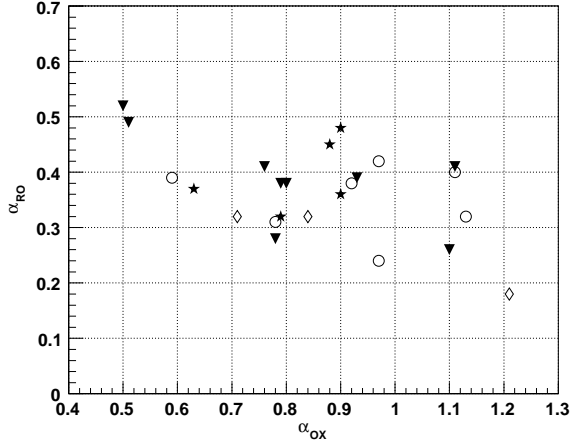


Fig. 4.— The overall spectral index α_{RO} vs. α_{OX} . The full symbols mark the sources which belong to the sample described in Sect.2. They are further divided into detected (stars) and non-detected sources (triangles). The open symbols represent all HBLs detected at VHE so far which belong not to the sample. They are further divided into sources with published fluxes (circles) and recent discovered sources without published γ -ray fluxes (diamonds).

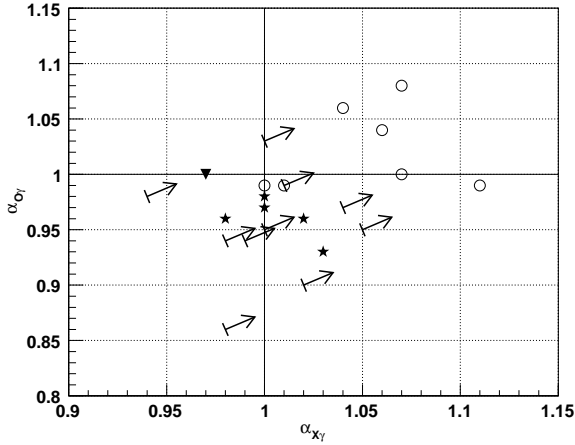


Fig. 5.— The overall spectral index $\alpha_{O\gamma}$ vs. $\alpha_{X\gamma}$. The arrows mark the u.l.s calculated in this work, while the stars indicate the detected sources that belong to the sample described in Sect.2. The open circles mark all are other detected HBL objects, where a flux at VHE γ -rays is already published.

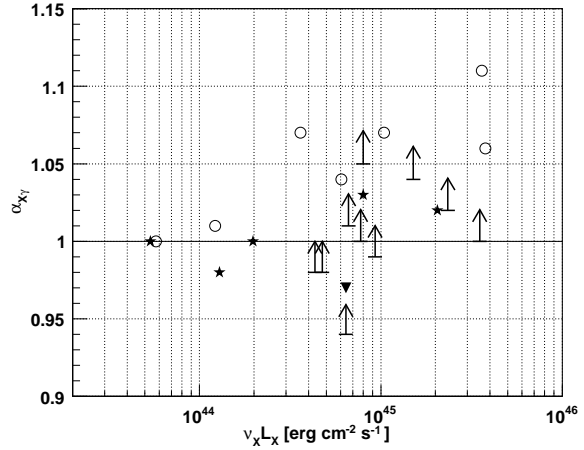


Fig. 6.— The overall spectral index $\alpha_{X\gamma}$ vs. the X-ray luminosity $\nu_X L_X$. The arrows mark the u.l.s calculated in this work, while the stars indicate the detected sources that belong to the sample described in Sect.2. The open circles mark all are other detected HBL objects, where a flux at VHE γ -rays is already published.

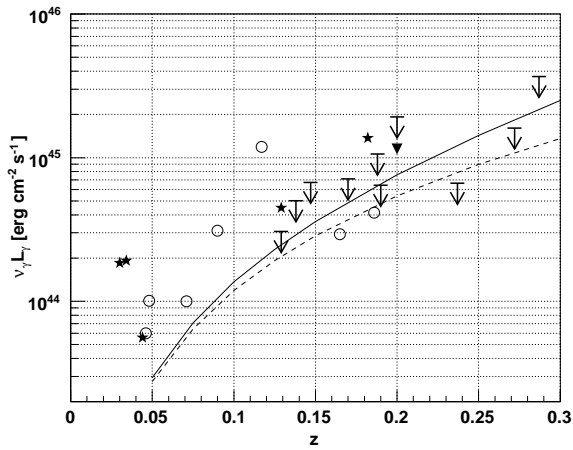


Fig. 7.— The γ -ray luminosity $\nu_\gamma L_\gamma$ vs. redshift. The arrows mark the u.l.s calculated in this work, while the stars indicate the detected sources that belong to the sample described in Sect. 2. The triangle marks 1ES 1011+49.6 if interpreted as a detection. The open circles mark all are other detected HBL objects, where a flux at VHE γ -rays is already published. The dashed line indicates a flux of $4.8 \times 10^{-12} \text{ erg cm}^{-2} \text{ s}^{-1}$ corresponding to $2 \mu\text{Jy}$ at 1 keV converted into the luminosity by only taking the distance into account. The solid line represents the same flux, taking into account also the absorption in the MRF at 200 GeV, when converting the flux into the intrinsic luminosity.